Study on Collapse Mechanism and Treatment Measures of Portal Slope of a High-speed Railway Tunnel

Guoping Hu (20201003@hncj.edu.cn)
Henan University of Urban Construction https://orcid.org/0000-0002-0833-8570
Yingzhi Xia
Henan University of Urban Construction
Lianggen Zhong
Changjiu Intercity Railway Co., Ltd
Xiaoxue Ruan
Henan University of Urban Construction
Qingguo Wang
Henan University of Urban Construction

Research Article

Keywords: Open cut tunnel, Slope deformation, Rainfall, Finite element method, Stabilization treatment, Field monitoring

Posted Date: February 1st, 2022

DOI: https://doi.org/10.21203/rs.3.rs-1210915/v1

Abstract

The slope of an open cut tunnel is located above the exit of the Leijia tunnel on the Changgan high-speed railway. During the excavation of the open cut tunnel foundation pit, the slope slipped twice, a large landslide of 92500 m³ formed. The landslide body and unstable slope body not only caused the foundation pit of the open cut tunnel to be buried and the anchor piles to be damaged but also directly threatened the operational safety of the later high-speed railway. Therefore, to study the stability change in the slope of the open cut tunnel under heavy rain and excavation conditions, a 3D numerical calculation model of the slope is carried out by Midas GTS software, the deformation mechanism is analyzed, anti-sliding measures are proposed, and the effectiveness of the anti-sliding measures is analyzed according to the field monitoring results. The results show that when rainfall occurs, rainwater collects in the open cut tunnel area, resulting in a transient saturation zone on the slope on the right side of the open cut tunnel, which reduces the shear strength of the slope soil; the excavation at the slope toe reduces the anti-sliding capacity of the slope toe. Under the combined action of excavation and rainfall, when the soil above the top of the anchor pile is excavated, two potential sliding surfaces are bounded by the top of the excavation area, and the shear outlet is located at the top of the anchor pile. After the excavation of the open cut tunnel, the potential sliding surface is mainly concentrated at the lower part of the downhill area, and the shear outlet moves down to the bottom of the open cut tunnel. Based on the deformation characteristics and the failure mechanism of the landslides, comprehensive control measures, including interim emergency mitigation measures and long-term mitigation measures, are proposed. The field monitoring results further verify the accuracy of the anti-sliding mechanism analysis and the effectiveness of anti-sliding measures.

1 Introduction

Rainfall and excavation are two main factors leading to landslides. Slope excavation rapidly adjusts the stress in the soil, causing some of the soil to yield, and cracks gradually appear or original cracks expand. The existence of cracks facilitates the infiltration of rainwater, and the infiltrated rainwater saturates the soil, increase the amount of rainwater infiltration into the slope, increase the unit weight of the slope soil, reduce the shear strength, and further reduce the stability of the slope. (Lin et al. 2018, Wang et al. 2013). The slope of Chenjiapo tunnel portal is affected by the combined action of soil excavation and rainfall, resulting in large-scale landslide, resulting in the tunnel portal being buried and had to be reinforced again (Hou et al. 2021). From May to July 2020, many areas in southern China experienced high rainfall, resulting in geological landslide disasters in many projects under construction in mountainous areas (Wei et al. 2020).

Many factors lead to slope instability, such as excavation, rainfall, reservoir storage, and earthquakes, and rainfall is one of the most important factors (Li et al. 2016, Sun et al. 2019, Zhang et al. 2015). Relevant research results show that nearly 90% of landslides in China are caused by rainfall or water level changes (Miao et al. 2017, Zeng et al. 2017). The influence of rainfall on slope stability is a primary research focus. Many physical test methods and numerical simulation methods are used to explore the

infiltration patterns of rainwater on slopes, the dynamic relationship between rainfall and the slope safety factor, and the influence of rainfall on slope deformation (Chen et al. 2018, Li et al. 2016, Sun et al. 2021).

Although rainfall is one of the main causes of slope instability, the natural slope is still in a stable state even after many years of rainfall before being disturbed artificially. In fact, when the slope is artificially disturbed, the vegetation on its surface or the soil layer with good water blocking effect will be damaged, accelerating the infiltration of rainwater. The above research results show that when slopes are affected by excavation and rainfall, its instability mechanisms become very complex, and the corresponding treatment measures are difficult to determine; this difficulty not only causes economic losses but also threatens people's lives and property safety (Gao et al. 2020, He et al. 2021, He et al. 2019, Zhu et al. 2019). Especially for the slope at the tunnel entrance, the tunnel construction needs to be carried out after the slope reinforcement is completed, which will disturb the slope toe again, and its deformation mechanism is more complex, which needs to be further studied.

Leijia tunnel of Changgan high-speed railway is located in an area with abundant rainfall and high weathering degree of mountains. In this paper, taking the slope at the exit of Leijia tunnel as an example, by means of field investigation, numerical analysis and field monitoring, this paper puts forward the optimal treatment measures based on the analysis of the instability mechanism of the slope, and evaluates the effectiveness of the reinforcement measures through the field monitoring data, so as to provide reference for relevant projects.

2 Study Area

2.1 Location of the Study Site

The Changgan high-speed railway from the Nanchang railway station to the Ganzhou west station, which construction period is from December 2014 to December 2019, is located in mid-southern Jiangxi Province, China. The total length of the Changgan high-speed railway is 416 km, of which the vast majority is in mountainous areas. The entrance and exit of Leijia tunnel studied in this paper are located in Qiaotou village, Jinchuan town, Xingan county (Fig. 1).

Xingan county is located in the transition zone between Jitai basin and Poyang Lake Plain. The whole county can be divided into four geomorphic types, namely, tectonic erosion low mountain terrain, tectonic erosion low mountain ~ hilly terrain, erosion denudation hilly mound terrain and valley alluvial plain terrain. Xingan County is an area prone to geological disasters, and the occurrence period of geological disasters is mainly concentrated in the period of continuous rainstorm in flood season. Geological disasters are mainly collapses, which are mainly characterized by great influence by climate differences and are closely related to typhoon and heavy rainfall, mainly in mountainous and hilly areas. In addition to natural factors, there are also human factors, such as engineering construction, slope cutting, etc.

2.2 Overview of the Slope Protection Design and Engineering Geology

The mileage of the Leijia tunnel exit (road and tunnel boundary) is DK36+001, the mileage of the boundary between the open cut tunnel and dark tunnel is DK35+971, and the length of the open cut tunnel section is 25 m; the slope ratio of the upward slope at the entrance of the tunnel is 1:1.25, which is protected by frame anchor bolts, and the mountain on the right side of the open tunnel is protected by anti-slide piles; the slope ratio above anti-slide piles is 1:1.5, and the primary slope is protected by anchor bolt frame beams; the first level slope is protected by anchor bolt frame beams, and the second level slope is protected by an arch skeleton, as shown in Fig. 2(a).

The groundwater in the project site is mainly quaternary void phreatic water. The surface layer of fully weathered granite has a loose structure and is saturated with water. The recharge source of groundwater is mainly rainfall, and the water level changes with the season. The bedrock fissure water is not developed.

According to the survey, the surface of the site is distributed with quaternary eluvial deluvial strata, and the underlying bedrock is Proterozoic phyllite and late yanshanian granite. The details of the strata from top to bottom according to their age and genesis are as follows: quaternary holocene eluvial diluvium, silty clay, fully weathered granite, fully weathered phyllite, highly weathered phyllite and weakly weathered phyllite, as shown in Fig. 2(b).

2.3 Initial Reinforcement Scheme for the Slope

The soil mass at the tunnel portal is excavated in two steps. The first step is to excavate the slope soil above the top of the anchor pile, and the second step is to excavate the soil mass of the open cut tunnel foundation pit, as shown in Fig. 2. In the first excavation, the slope is reinforced in two stages, the slope ratio is 1:1.5, and the heights of both benches are 8 m. A platform with a width of 2m is designed between the two slopes. The slope surface is protected by a mortar anchor rod, and the length of the anchor rod is 8 m. The right side of the open cut tunnel foundation pit is reinforced with anchor piles, the plane size of the piles is 2*2.25 m, and the length of the piles is 16 m, as shown in Fig. 2.

2.4 Deformation and Instability Process of the Slope

The slope project at the exit of Leijia tunnel has been under construction since February 2016. During construction, the surrounding rock at the exit slope of the tunnel was extremely broken and was mainly composed of silty clay, a locally fine sand layer, and rich groundwater, and the left slope was wet from the excavation. To ensure the stability of the slope, temporary support works of the slope and front slope were carried out, and the anti-sliding pile hole was excavated at the position of the primary platform. In April 2016, heavy rainfall occurred in the area where the tunnel was located, and the originally wet slope began to seep. In particular, the area 5 m above the secondary platform on the right slope of section DK36 + 005 became a water inflow area after rain (Fig. 3a). The whole front slope collapsed and fluid gushed out, and a tensile fracture with a width of approximately 80 cm appeared at the rear edge of the landslide. The constructed anti-sliding pile hole on the right side of the open cut tunnel was buried by a landslide (Fig. 3b). The landslide mass is tongue shaped on the plane, approximately 120 m in length and 25 m in width; the area of the landslide body is approximately 9100 m^2(Fig. 3c).

From April 2016 to March 2017, slope reinforcement was carried out at the site, and no tunnel excavation was carried out. On March 1, 2017, the construction of the anti-slide piles on the upper part of the slope and the adjacent tunnel was completed. On March 3, 2017, the dark part of the tunnel was excavated for the first time, and the first slab lining was constructed on April 18, 2017. From approximately 4:00 p.m. on April 19, 2017 to 6:15 a.m. on April 20, 2017, there was heavy rainfall (heavy rain). At 6:40 a.m., it was discovered that the soil collapsed between the bored cast-in-place piles on the right side of the exit open cut tunnel (Fig. 4a). Then, large cracks on the slope (Fig. 4b) and obvious displacement of the bored cast-in-place pile on the right side of the open cut tunnel were found (Fig. 4c).

3 Numerical Simulation

To further explore the deformation mechanism of the slope and explore appropriate slope reinforcement measures, numerical calculations were used to analyze the deformation, stability and seepage field of the slope. Midas GTS numerical analysis software is used for numerical analysis and calculation.

3.1 Model Description

The numerical model is established according to the actual landform and geological conditions of the slope, as shown in Fig. 5. The calculation model contains 75290 nodes and 126948 elements. The rock and soil are simulated by Mohr Coulomb elastic-plastic constitutive model, and the pile is simulated by elastic constitutive model. Solid element is adopted for rock and soil, beam element is adopted for pile, and beam element and truss element are adopted for anchorage section and free section of anchor cable respectively.

In the Midas GTS model, the groundwater level is defined at the interface of the eluvial layer and weathered phyllite (Ye et al. 2021). Rainfall simulation is realized by applying surface flow on the upper surface of the model, and the rainfall value is set according to the results of on-site monitoring. The saturated permeability coefficient of the eluvial layer is 5×10^{-5} m/s, and the saturated permeability coefficient of weathered phyllite is 1×10^{-5} m/s.

The boundary conditions of the model are as follows: the four sides restrict the displacement in the horizontal direction, the bottom restricts the displacement in the vertical direction, and restricts the rotation of the pile around its axis. (Li et al. 2020). The physical and mechanical parameters of the soil and rock are obtained according to the laboratory test, as shown in Table 1.

Table 1
Main parameters of the materials used in the numerical model

Material	Unit weight (kN/m^3)	Cohesion (kPa)	Internal friction angle(°)	Young's modulus (MPa)	Poisson's ratio	Permeability coefficient (m/s)
Eluvial layer	20	25	19	12.5	0.36	5×10^{-5}
Weathered phyllite	22	37	35	26.5	0.3	1×10^{-5}
Weakly weathered granite	23	150	45	95	0.32	6×10^{-4}
Anchor cable	78	/	/	1.95×10^{6}	/	/
Concrete	25	/	/	3.15×10^{4}	/	/

The calculation process of the numerical model is determined according to the actual construction steps on site. The calculation process is divided into four steps. First, the initial stress of the natural slope is simulated. The second step is to apply rainfall to the excavated slope surface and calculate the slope deformation under rainfall conditions (Bo et al. 2019, Greco et al. 2021). The third step is to construct anti-slide measures and excavate the soil of the open tunnel foundation pit. The fourth step is to apply rainfall again and calculate the deformation of the slope after the rainfall. The rainfall value applied on the model boundary is selected according to the actual rainfall value.

3.2 Analysis of the Seepage Field of the Slope

Figure 6(a) shows that on mountains, when rainfall occurs, the water on the slope converges along the slope to the area where the tunnel is located while seeping downward. The field survey shows that there are several water outlets at the lower part of the slope when continuous rainfall occurs, which indicates that the calculated results are basically consistent with the actual results. Figure 6(b) shows the distribution of the transient saturation zone of the slope on April 10 and 26. The figure shows that after three consecutive days of rainfall, several saturation zones appear on the slope, and the saturation areas are mainly concentrated in the open cut tunnel area and its upper area, which is basically consistent with the sliding area found on site.

3.3 Analysis of the Displacement Field of the Slope

Figure 7 shows the overall displacement contour distribution of the slope after being affected by excavation and rainfall. Figure 7(a) shows the deformation of the slope when the topsoil in the location of the open cut tunnel is excavated. At this time, the area of slope deformation is mainly near the open cut tunnel, the maximum displacement is 11.91 cm, and the deformation in other areas is small. Figure 7(b) adds the rainfall calculation based on the first excavation calculation, and the maximum displacement value of the slope is 51.31 cm, which is significantly larger than that without rainfall, and the deformed area is also enlarged; its shape is basically the same as that of the site survey in Fig. 4.

Figure 7(c) shows the deformation of the slope after the anchor pile is constructed and the second excavation is carried out. The maximum displacement of the slope is 63.52 cm, which is slightly larger than that in Figure 7(b). Figure 7(d) shows the deformation of the slope after rainfall again, and the maximum displacement of the slope is 98.65 cm.

Compared with the calculation results of the above four steps, both the soil excavation and rainfall have a great impact on the slope deformation. The increases in the extreme values of slope deformation caused by the two soil excavations are 11.91 cm and 12.21 cm, respectively, and the increases in the extreme values of slope deformation caused by the two rainfall events are 39.4 cm and 35.13 cm, respectively. The impact of rainfall on the slope deformation is more significant after the topsoil is excavated.

3.4 Analysis of the Distribution of Plastic Zone

To assess the instability of the slope under different working conditions, the main sliding section is selected to analyze the distribution of the soil plastic zone (Sheng et al. 2002). Fig. 8(a) shows that within the first excavation, due to rainfall infiltration and soil excavation, an obvious plastic zone appeared on the upper layer of the slope, and two potential sliding surfaces appeared, which basically matched the field monitoring results in Fig. 4. Fig. 8(b) shows the distribution of the plastic zone of the slope after the secondary excavation of the soil. The figure shows that the position of the plastic zone of the slope is mainly concentrated in the toe area, which is deeper than the position of the plastic zone calculated by the first excavation.

4 Triggering Mechanism

According to the field survey results and numerical analysis results, the factors affecting the stability of tunnel portal slopes are analyzed and discussed.

4.1 Continuous Rainfall

The studied region has a subtropical monsoon climate and abundant rainfall. The mean annual precipitation in Xingan County is 1678.9 mm. In April 2016 and 2017, heavy rainfall occurred continuously in the survey area, and the total rainfall in April 2016 and 2017 reached 354.4 mm and 151.4 mm, respectively (Fig. 9a). Because the permeability coefficient of each layer of soil in the site is different, and the permeability coefficient of surface soil is less than that of underlying bedrock, the rainfall infiltrated water will be stored in the upper weathered soil layer, saturating the weathered soil layer and increasing the unit weight, as shown in Fig. 6(b) and Fig. 9(b).

The shear strength of the soil at the interface between fully weathered phyllite and fully weathered granite decreases abruptly after being soaked in rain, thereby forming a weak surface and reducing the stability of the slope, which creates convenient conditions for the sliding of the slope.

4.2 Excavation Activities

In the first stage, the soil mass of the slope above the top of the anchor pile was excavated, and several anchor piles were excavated, as shown in Fig. 9(b). During this period, no effective protection or drainage measures were formed on the slope surface, and the excavation of large-scale anchor piles further damaged the anti-sliding capacity of the slope toe. At the same time, slope excavation destroyed the vegetation, increased the infiltration of rainwater, and accelerated the formation of a soft layer in the soil, resulting in a collapse of the slope in April 2016, as shown in Fig. 3. The second stage of excavation was executed after some reinforcement measures were completed, and the excavated area was mainly the soil of the open cut tunnel. This stage was affected by the accumulation of excavation deformation generated in the previous stage, and the anti-sliding ability of the original anchor pile was insufficient, which led to the stability of the soil in the lower part of the slope again.

5 Stabilization Treatment

The methods of slope treatment generally include reducing the sliding force and increasing resistance, or both. For landslides caused by artificial interference, due to the requirements for the protection of machinery, equipment and personnel at the construction site, temporary reinforcement is carried out the first time the landslide occurs, and then permanent reinforcement measures are constructed.

5.1 Temporary Remediation Measures

Back-pressure backfilling is an effective temporary treatment measure that can effectively improve the resistance of the slope toe; therefore, the emplacement of temporary protective measures is also designed from these two aspects. According to the above analysis, excavation and rainfall are the two main sliding-inducing factors, so back-pressure backfilling at the toe of the slope is carried out for the first time that the slope collapses (Fig. 11a). At the same time, to prevent rainwater from infiltrating and weakening the soil, multiple intercepting ditches and drainage ditches are excavated at the open line of the slope to ensure that the ground rainwater can be drained in time (Fig. 11b), and M7.5 mortar is used to block the cracks. Furthermore, the damaged shotcrete on the slope surface should be removed, respraying measures should be carried out; the inclined drainage holes on the slope should be encrypted at a depth of 10 m, and perforated corrugated pipes or PVC pipes should be inserted into the drainage holes.

5.2 Long-term Remediation Measures

The permanent reinforcement measures shall be designed according to the above numerical calculation results and field survey results. According to the above calculation and analysis results, there are two potential sliding surfaces on the slope, and reinforcement measures should be designed for the two potential sliding areas. In view of the construction flexibility of anti-slide piles, different forms of anti-slide piles are designed at the middle and toe of the landslide according to the anti-slide requirements, and mortar anchor bolts are constructed on the slope.

The designed anti-slide rigid frame pile is shown in Fig. 10. Its specific parameters are as follows: the pile material is C35 concrete, the pile length is 24 m and is composed of two piles with a single length of 12 m, the diameter of the pile is 2 m, the pile spacing between the two piles is 2 m in the transverse direction and 5 m in the longitudinal direction, and a crown beam is set at the top of the pile; the thickness of the crown beam is 1.5 m.

As the rainfall in the survey area is large and the soil is always wet, the construction of manual hole digging piles is difficult, and large deformation occurs at the slope toe after secondary excavation, so the anti-slide pile at the slope toe is optimized. The specific design of the anchor pile is as follows: the anchor pile is designed as a circular bored cast-in-place pile with a pile diameter of 2 m, a pile spacing of 3 m, a pile length of 18 m, and a crown beam with a thickness of 1.5 m is set on the top of the pile. The length of the anchor cables is 25 m, the longitudinal spacing is 3 m, the length of the anchor section is 15 m, the inclination angle is 25 degrees, and the prestress is applied at 300 kN, as shown in Fig. 11c.

CFG piles are added to the tunnel base of section DK35+971~DK36+001 for reinforcement, with a pile diameter of 0.5 m, spacing of 1.6 m and reinforcement width of 15 m. The pile length of section DK35+971~976 is 8 m, and the pile length of section DK35+976~DK36+001 is 10 m.

6 Monitoring Instrumentation

From April 2016 to March 2017, the slope was under reinforcement construction, no effective monitoring network was formed, and field monitoring of the study area began in July 2017. The monitoring system includes thirty surface displacement measuring points. Seven displacement monitoring points are arranged on the upper part of the landslide mass, thirteen displacement monitoring points are arranged on the lower part, and ten monitoring points are arranged on the pile top beam, as shown in Fig. 12. The monitoring time intervals of the surface displacement are generally 1 day.

Affected by the construction of the slope reinforcement project, the lower slope monitoring point did not obtain monitoring data from July 19 to August 12, 2017. At this stage, the slope above the anti-slide pile was basically not deformed, and the deformation of the remaining parts is as follows.

Figure 13 shows the displacement of the anti-slide pile top beam in both the vertical railway strike direction and settlement. During the whole monitoring process, the deformation of the anti-slide pile itself was relatively small, the maximum horizontal displacement value of its top was 3.36 cm, and the maximum settlement value was only 0.52 cm.

Figure 14 shows that the deformation of the upper part of the slope is obviously smaller than that of the lower part. The lower slope has a large deformation, the maximum horizontal displacement value is 13.11 cm, and the maximum settlement value is 11.76 cm. During the monitoring process, there were two obvious increases in the data, which occurred from August 23 ~ August 25 and from October 11 ~ October 13. According to the meteorological monitoring records of the site, the daily rainfall on August 24

reached 56.8 mm, and the cumulative rainfall from October 11 to 13 reached 56.6 mm. Clearly, rainfall has a great influence on the deformation of the tunnel portal slope.

Compared with the sudden increase in the two displacements, the sudden increase in October is much larger than that in August. Further analysis combined with the field construction records shows that the back-pressure soil was not excavated in August, but the back-pressure soil was excavated in October; the anchor cable construction of the anchor pile was not completed, and the anti-slide force was still insufficient. Based on the analysis of the above two factors, the main cause of slope deformation is rainfall, but the reinforcement conditions determine the magnitude of the deformation. After anchor cable construction is completed, the slope tends to stabilize.

Figure 14 shows that the slope was basically stable on November 1, and the on-site slope has not been deformed thus far, indicating that the abovementioned treatment measures are basically effective.

7 Conclusions

The deformation and failure of the slope at the exit of the Leijia tunnel induced during the construction of the Changgan high-speed railway in Jiangxi Province, China, was investigated, and the optimal reinforcement measures are proposed. Through the research of this paper, the following conclusions can be drawn from this case study:

(1) The studied slope is mainly composed of fully weathered granite and phyllite, and the rock mass is broken and has low strength. The slope experienced heavy rainfall before collapse, and the slope was in a saturated state, which reduced the shear strength of the soil. In the process of excavating slopes and open cut tunnel foundation pits, the construction speed was fast, and the originally designed reinforcement measures were not implemented in time. The combination of excavation and rainfall triggered the landslides, although rainfall played the leading role.

(2) According to the simulation results, after rainfall began, the rainwater on the hillside converged to the tunnel. With the continuation of rainfall, a transient saturation zone was observed on the slope near the open cut tunnel. Due to the influence of rainwater and excavation, several obvious plastic zones appeared in the slope.

(3) According to the numerical analysis and field investigation results, it is necessary to set anti-slide piles in the middle and bottom of the slope and construct mortar anchor bolts on the slope. After the slope collapses, there is a continuous sliding surface in the slope body. The construction of anti-sliding measures only in the middle of the landslide have difficulty ensuring the stability of the lower slope. It is also necessary to strengthen the anchor pile at the slope toe to ensure slope stability.

Declarations

Acknowledgments

The authors acknowledge the financial support received from the Key Scientific Research Project of Colleges and Universities in Henan Province under Grant 22B580001 of the Education Dept., Henan Province.

Competing Interests

The authors have no relevant financial or non-financial interests to disclose.

References

1. Bo A, Chun Z, Kuiming L, Sitong L, Zhigang T, Haipeng L, Haoran Y (2019) The influence of rainfall on landslide stability of an open-pit mine: The case of haizhou open-pit mine. Geotech Geol Eng 37:3367–3378. 10.1007/s10706-019-00851-y
2. Chen M-l, Lv P-f, Zhang S-l, Chen X-z, Zhou J-w (2018) Time evolution and spatial accumulation of progressive failure for xinhua slope in the dagangshan reservoir, southwest china. Landslides 15:565–580. 10.1007/s10346-018-0946-8
3. Gao Y, Li B, Gao H, Chen L, Wang Y (2020) Dynamic characteristics of high-elevation and long-runout landslides in the emeishan basalt area: A case study of the shuicheng “7.23”landslide in guizhou, china. Landslides 17:1663–1677. 10.1007/s10346-020-01377-8
4. Greco R, Comegna L, Damiano E, Marino P, Olivares L, Santonastaso GF (2021) Recurrent rainfall-induced landslides on the slopes with pyroclastic cover of partenio mountains (campania, italy): Comparison of 1999 and 2019 events. Eng Geol 288:106160. https://doi.org/10.1016/j.enggeo.2021.106160
5. He K, Liu B, Hu X (2021) Preliminary reports of a catastrophic landslide occurred on august 21, 2020, in hanyuan county, sichuan province, china. Landslides 18:503–507. 10.1007/s10346-020-01566-5
6. He K, Ma G, Hu X, Luo G, Mei X, Liu B, He X (2019) Characteristics and mechanisms of coupled road and rainfall-induced landslide in sichuan china. Geomatics, Natural Hazards and Risk 10:2313–2329. 10.1080/19475705.2019.1694230
7. Hou TS, Duan X, Liu HY (2021) Study on stability of exit slope of chenjiapo tunnel under condition of long-term rainfall. Environ Earth Sci 80:1–14. https://doi.org/10.21203/rs.3.rs-176316/v1
8. Li Q, Wang YM, Zhang KB, Yu H, Tao ZY (2020) Field investigation and numerical study of a siltstone slope instability induced by excavation and rainfall. Landslides 17:1485–1499. 10.1007/s10346-020-01396-5
9. Li W, Liu C, Hong Y, Saharia M, Sun W, Yao D, Chen W (2016) Rainstorm-induced shallow landslides process and evaluation – a case study from three hot spots, china. Geomatics, Natural Hazards and Risk 7:1908–1918. 10.1080/19475705.2016.1179685
10. Li WC, Dai FC, Wei YQ, Wang ML, Min H, Lee LM (2016) Implication of subsurface flow on rainfall-induced landslide: A case study. Landslides 13:1109–1123. 10.1007/s10346-015-0619-9

11. Lin F, Wu LZ, Huang RQ, Zhang H (2018) Formation and characteristics of the xiaoba landslide in fuquan, guizhou, china. Landslides 15:669–681. 10.1007/s10346-017-0897-5
12. Miao F, Wu Y, Xie Y, Yu F, Peng L (2017) Research on progressive failure process of baishuihe landslide based on monte carlo model. Stoch Env Res Risk Assess 31:1683–1696. 10.1007/s00477-016-1224-8
13. Sheng Q, Yue ZQ, Lee CF, Tham LG, Zhou H (2002) Estimating the excavation disturbed zone in the permanent shiplock slopes of the three gorges project, china. Int J Rock Mech Min Sci 39:165–184. https://doi.org/10.1016/S1365-1609(02)00015-1
14. Sun H-y, Ge Q, Yu Y, Shuai F-x, Lü C-c (2021) A new self-starting drainage method for slope stabilization and its application. Bull Eng Geol Environ 80:251–265. 10.1007/s10064-020-01918-4
15. Sun H-Y, Pan P, Lü Q, Wei Z-L, Xie W, Zhan W (2019) A case study of a rainfall-induced landslide involving weak interlayer and its treatment using the siphon drainage method. Bull Eng Geol Environ 78:4063–4074. 10.1007/s10064-018-1365-8
16. Wang JJ, Liang Y, Zhang HP, Wu Y, Lin X (2013) A loess landslide induced by excavation and rainfall. Landslides 11:141–152. https://doi.org/10.1007/s10346-013-0418-0
17. Wei K, Ouyang C, Duan H, Li Y, Chen M, Ma J, An H, Zhou S (2020) Reflections on the catastrophic 2020 yangtze river basin flooding in southern china. The Innovation 1:100038. https://doi.org/10.1016/j.xinn.2020.100038
18. Ye F, Fu W-X, Zhou H-F, Liu Y, Ba R-J, Zheng S (2021) The “8·21” rainfall-induced zhonghaicun landslide in hanyuan county of china: Surface features and genetic mechanisms. Landslides 18:3421–3434. 10.1007/s10346-021-01722-5
19. Zeng L, Bian H-b, Shi Z-n, He Z-m (2017) Forming condition of transient saturated zone and its distribution in residual slope under rainfall conditions. Journal of Central South University 24:1866–1880. 10.1007/s11771-017-3594-6
20. Zhang M, Yin Y, Huang B (2015) Mechanisms of rainfall-induced landslides in gently inclined red beds in the eastern sichuan basin, sw china. Landslides 12:973–983. 10.1007/s10346-015-0611-4
21. Zhu L, Deng Y, He S (2019) Characteristics and failure mechanism of the 2018 yanyuan landslide in sichuan, china. Landslides 16:2433–2444. 10.1007/s10346-019-01262-z

Figures

Figure 1

Location of the study site in Jiangxi Province, China

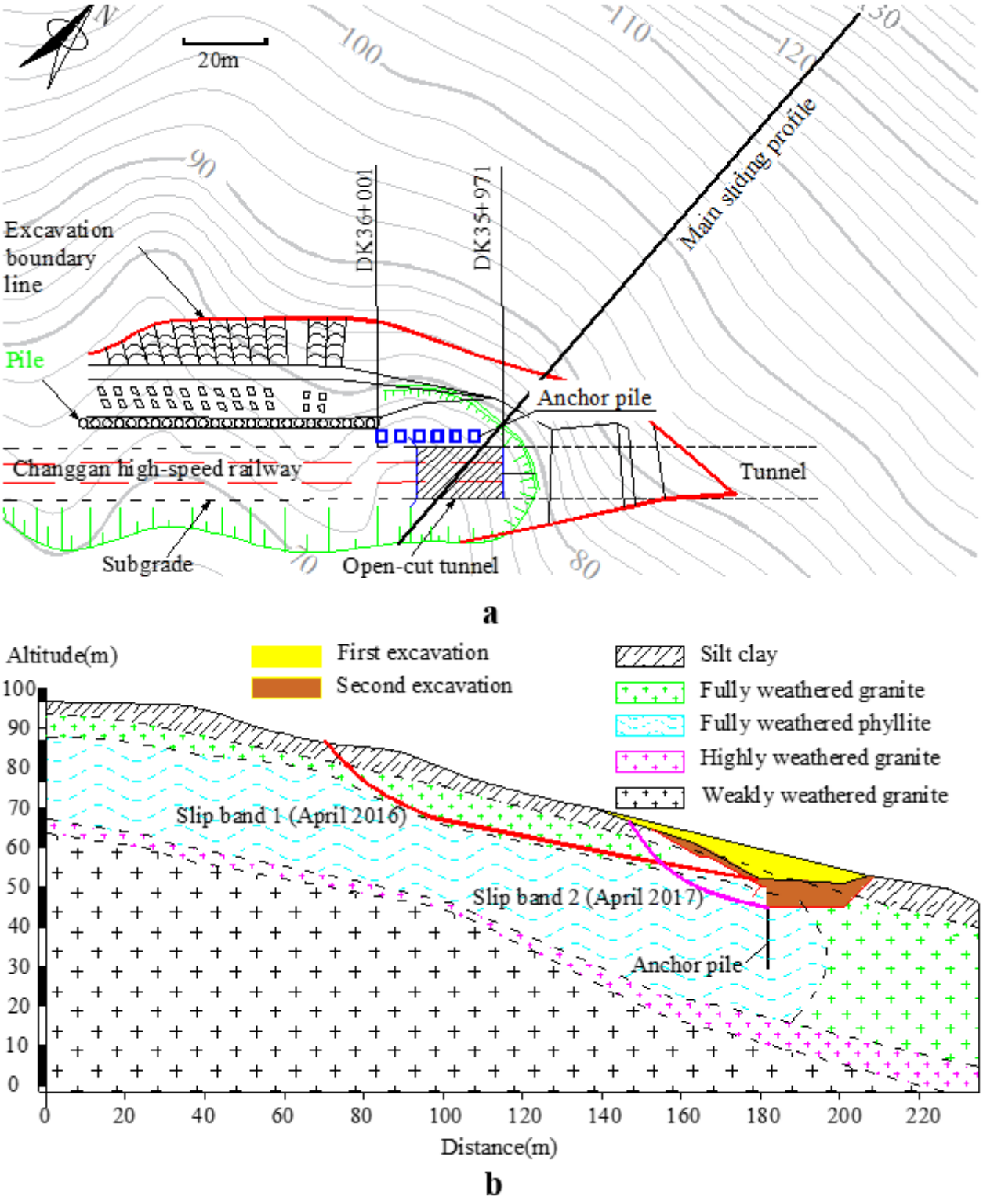

Figure 2

a Original design of the slope, **b** longitudinal section of the slope

a b

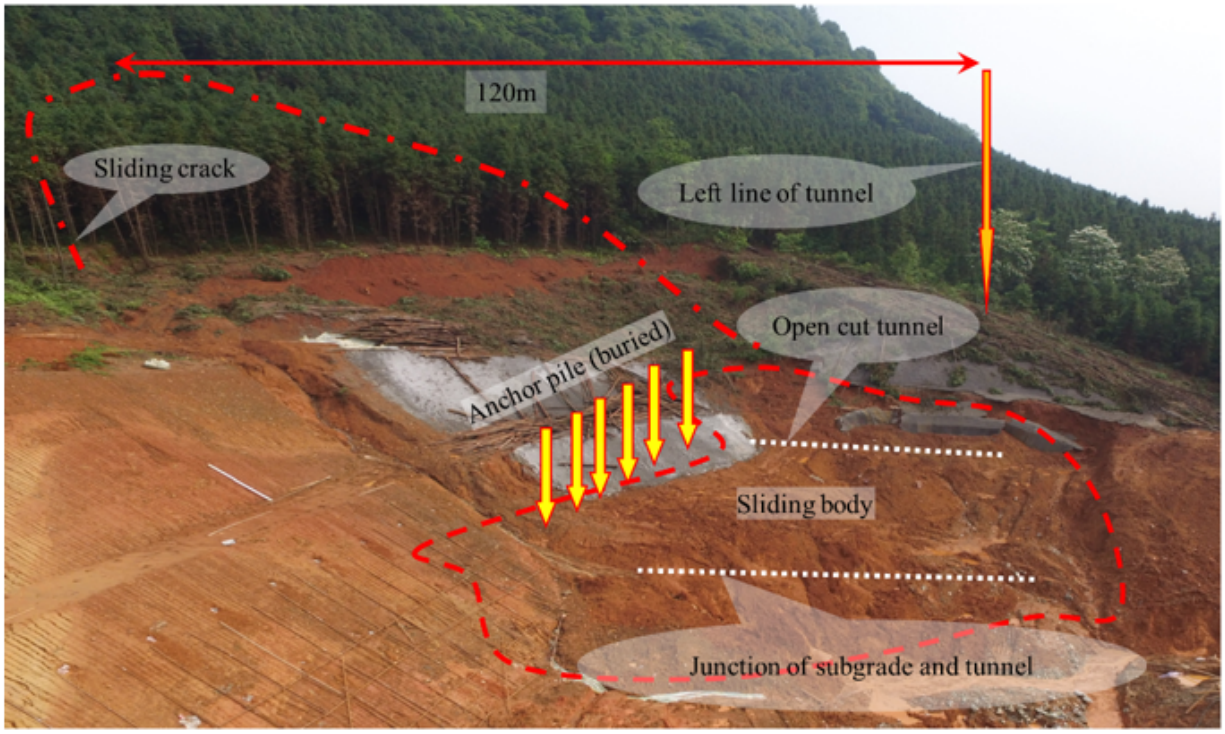

c

Figure 3

April 2016, **a** water inflow area, **b** tensile cracks at the trailing edge of the slope, **c** picture of the slope collapse

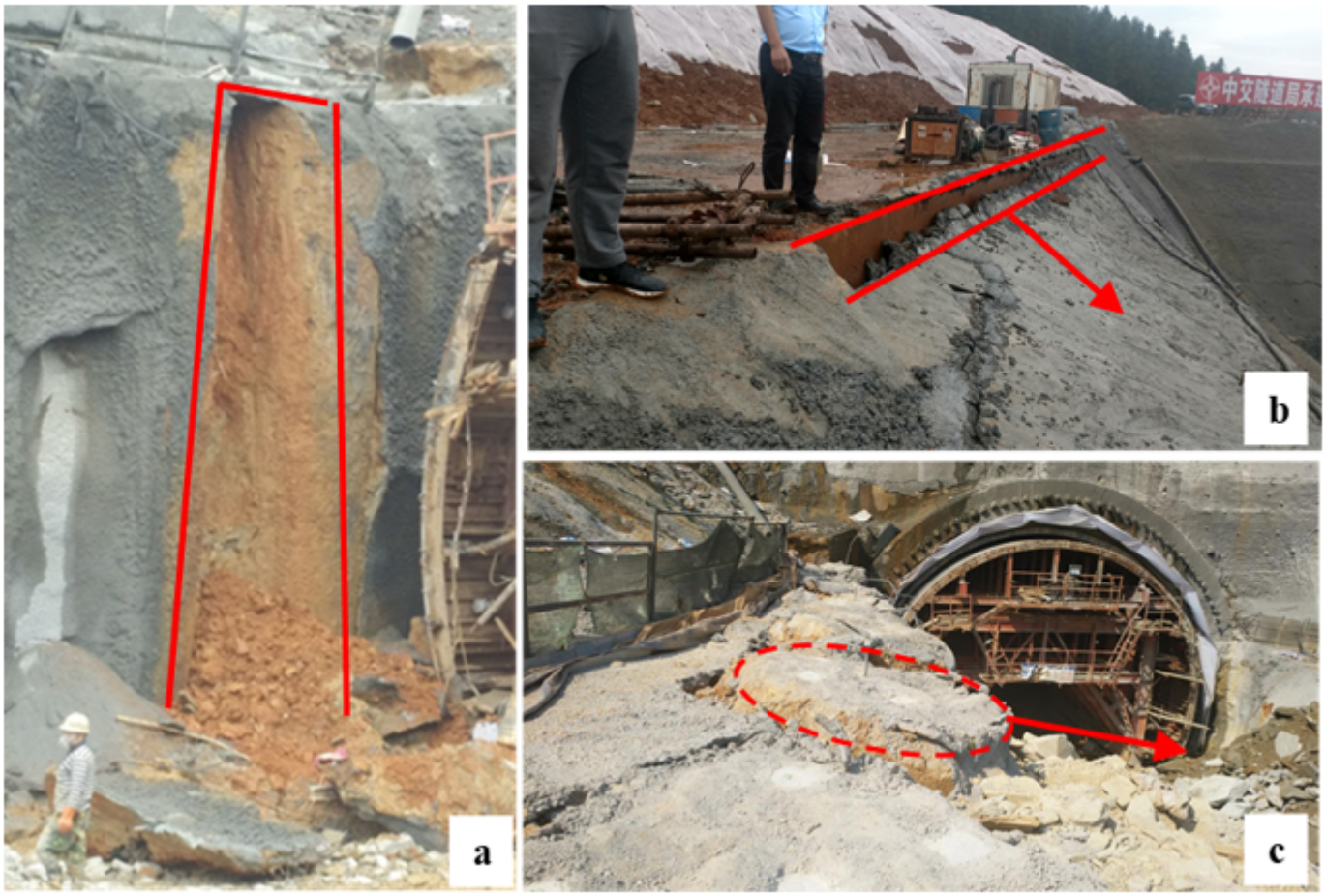

Figure 4

April 2017, **a** collapse of the soil between piles, **b** slope cracking, **c** lateral displacement of the pile

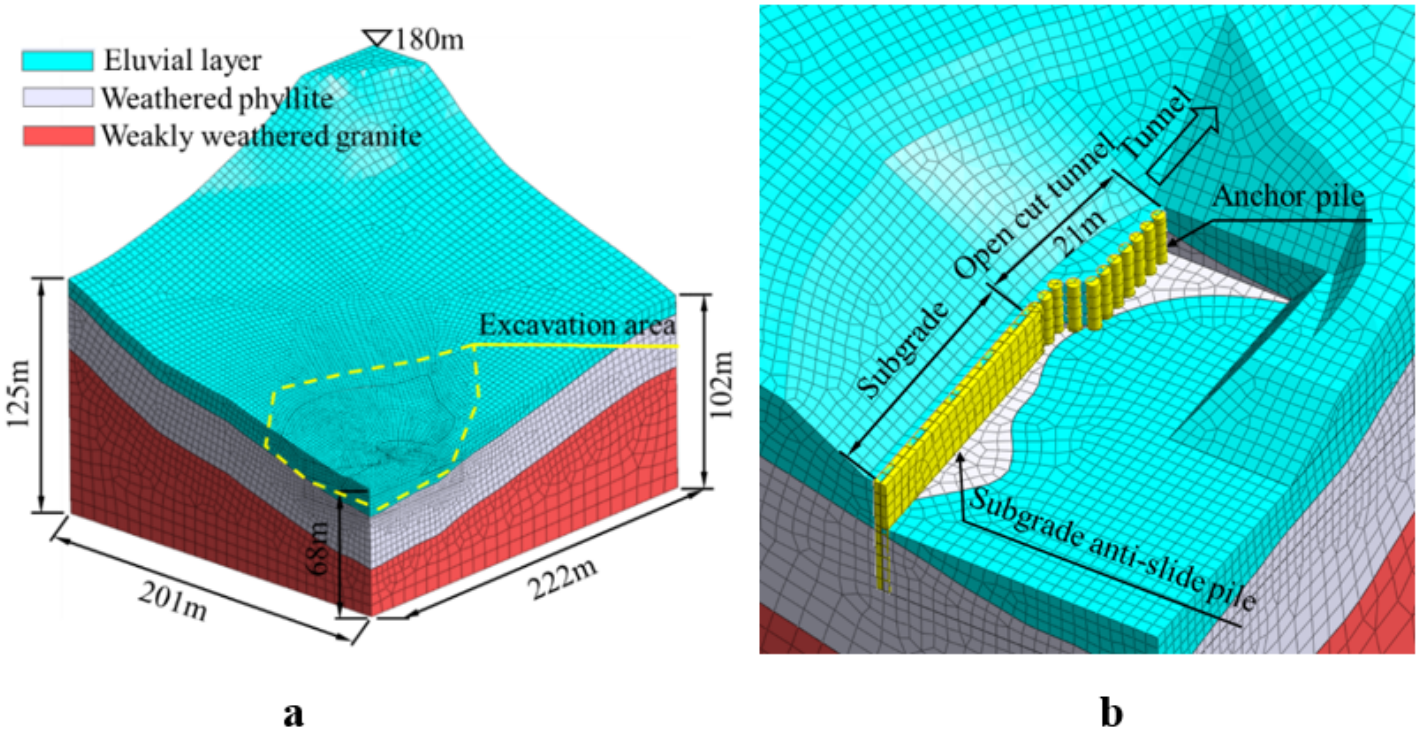

Figure 5

a Calculation model**, b** partial enlarged drawing of the excavation area

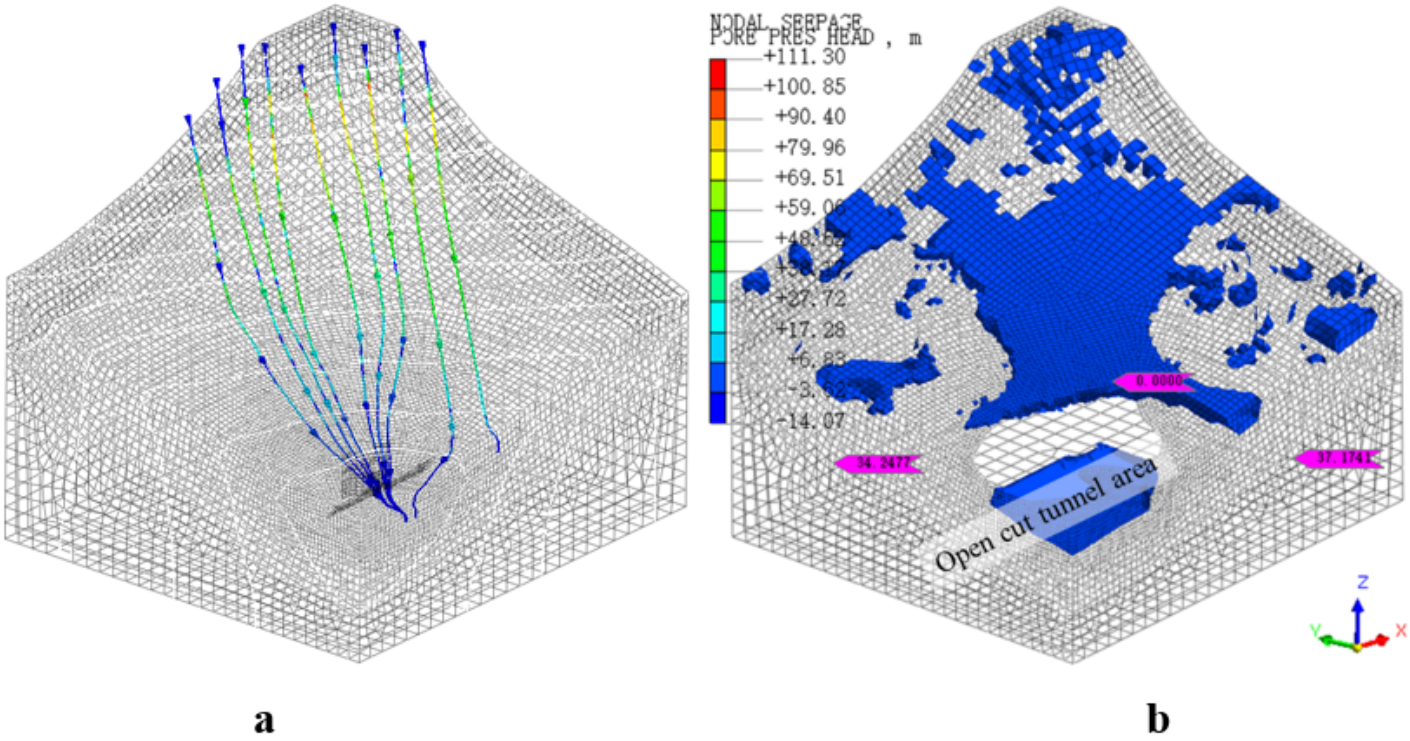

Figure 6

a Flow path diagram of water and **b** distribution of the transient saturation zone (2016/04/10)

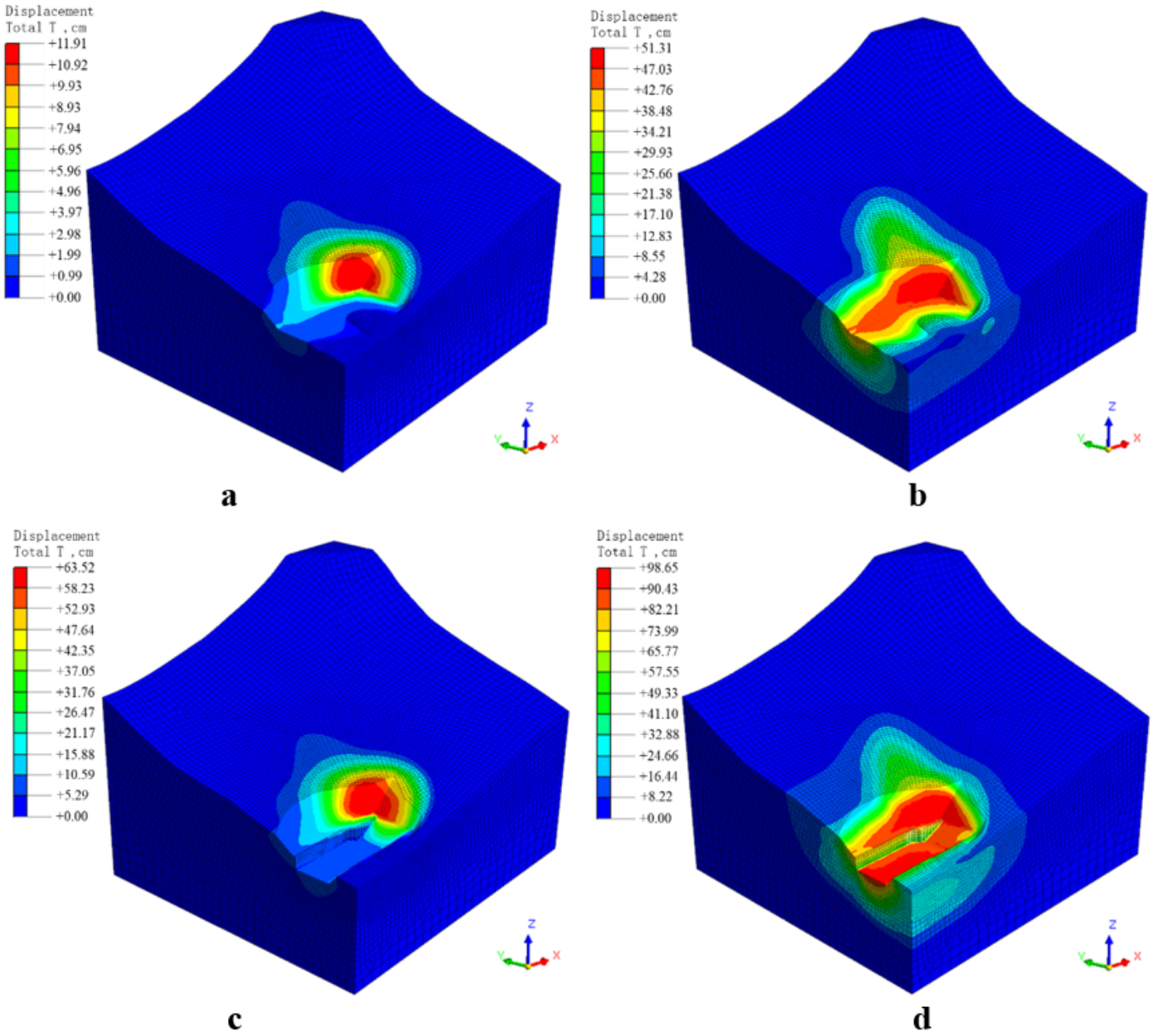

Figure 7

a Deformation of the slope after the first excavation, **b** deformation of the slope caused by rainfall after the first excavation, **c** deformation of the slope after the second excavation, **d** deformation of the slope caused by rainfall after the second excavation

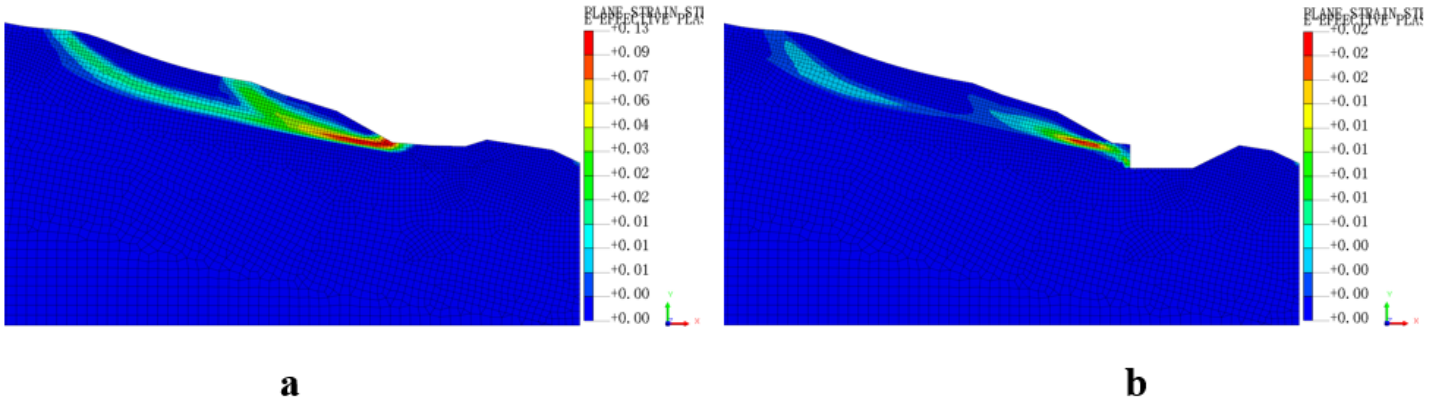

Figure 8

Variation in the plastic zone of the slope. **a** First excavation. **b** Second excavation

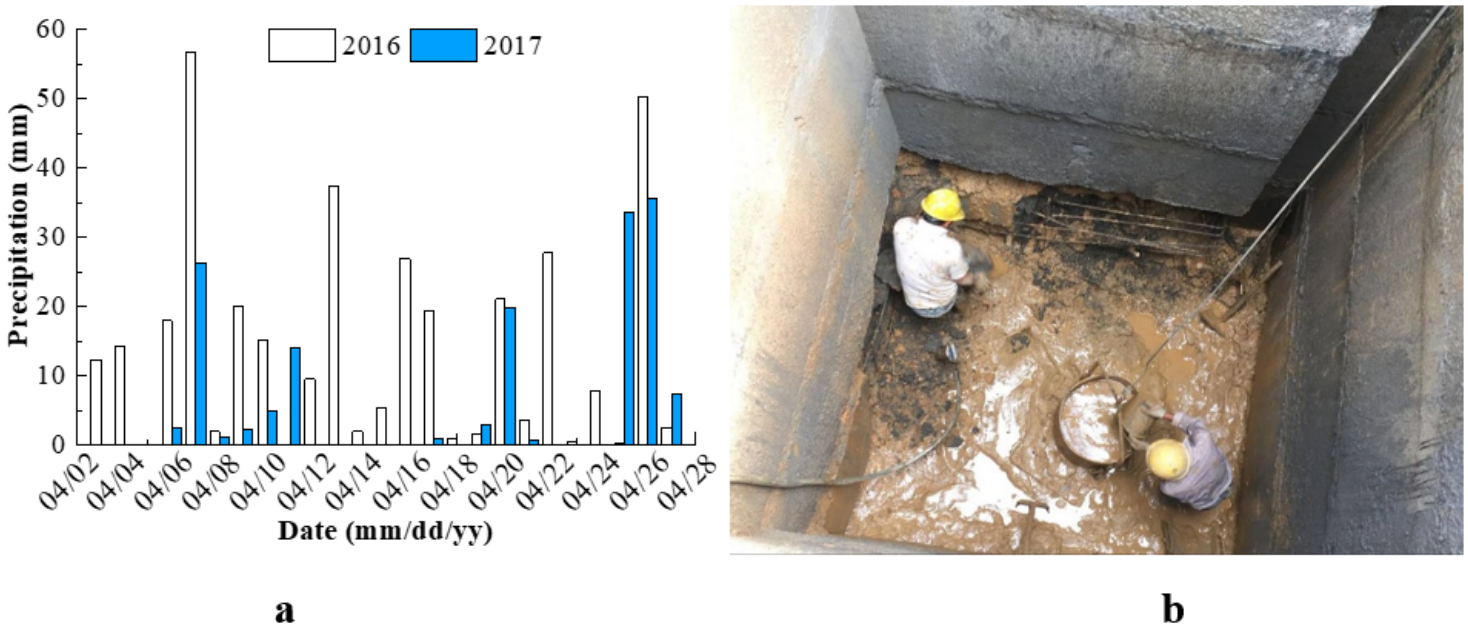

Figure 9

a Daily precipitation in the study area (2016 and 2017), **b** excavation of anchor piles

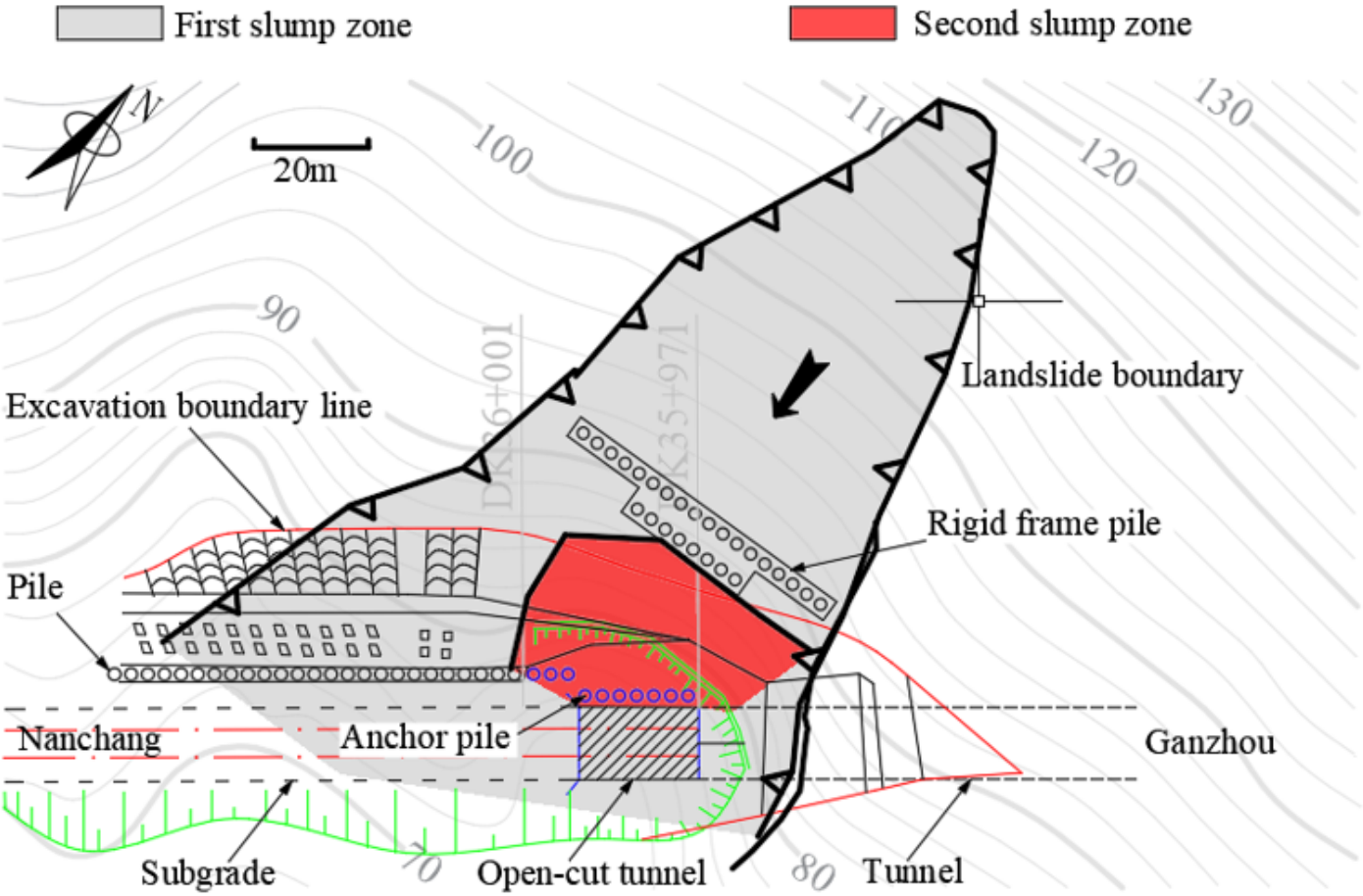

Figure 10

Design of reinforcement measures

Figure 11

Reinforcement: **a** earth and rock backfill, **b** interception and drainage measures, **c** addition of anchor piles

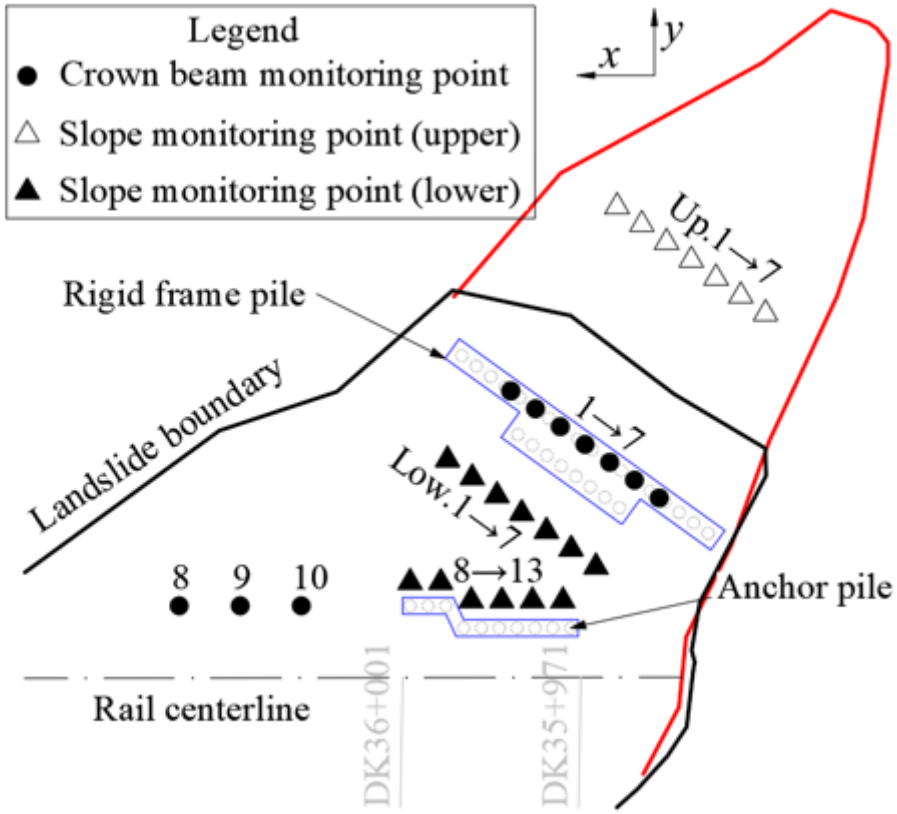

Figure 12

Layout of displacement monitoring points on slope and anti-sliding pile

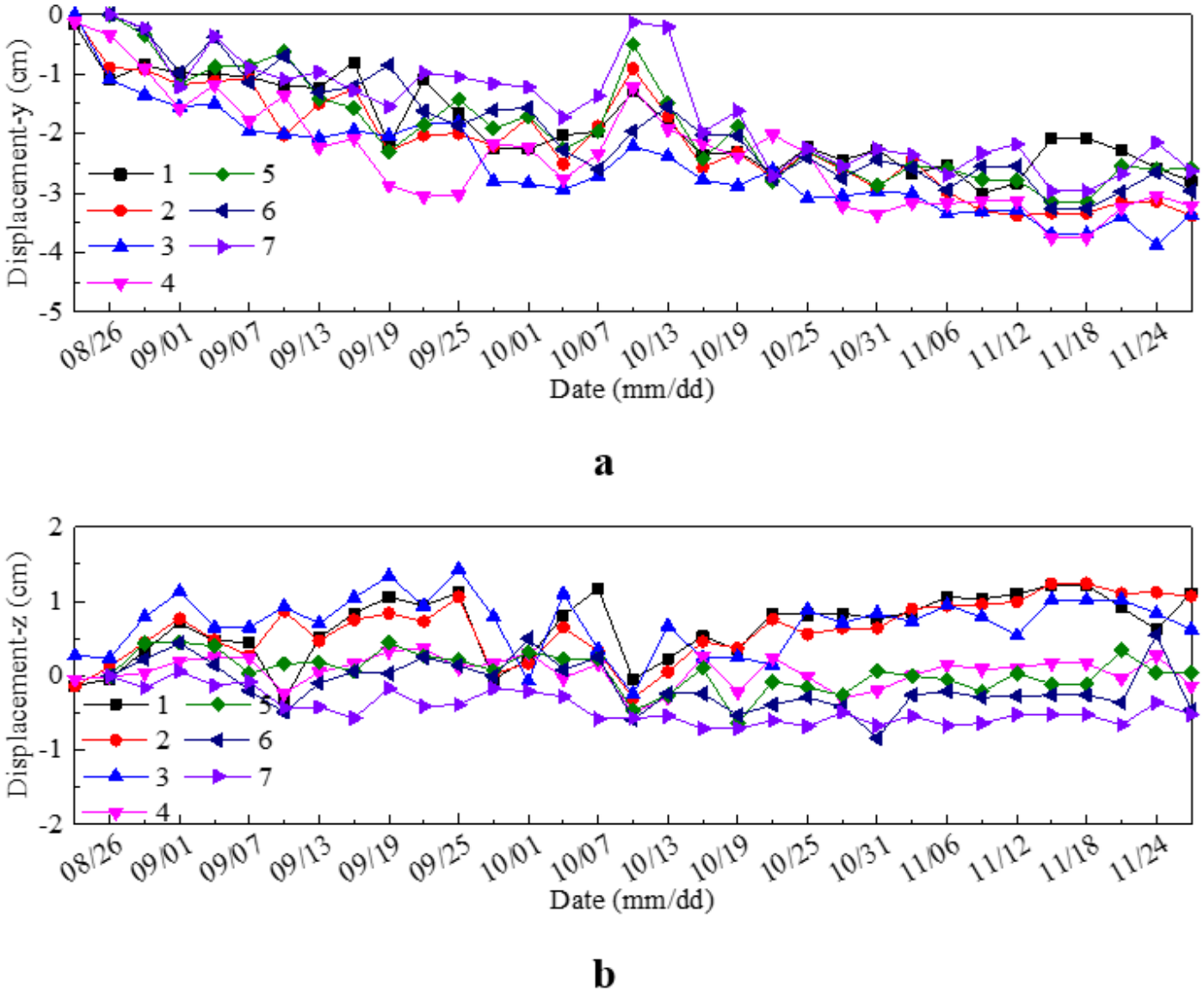

Figure 13

Monitoring results of the displacement of the top beam: **a** displacement vertical railway strike direction (y), **b** settlement deformation (z)

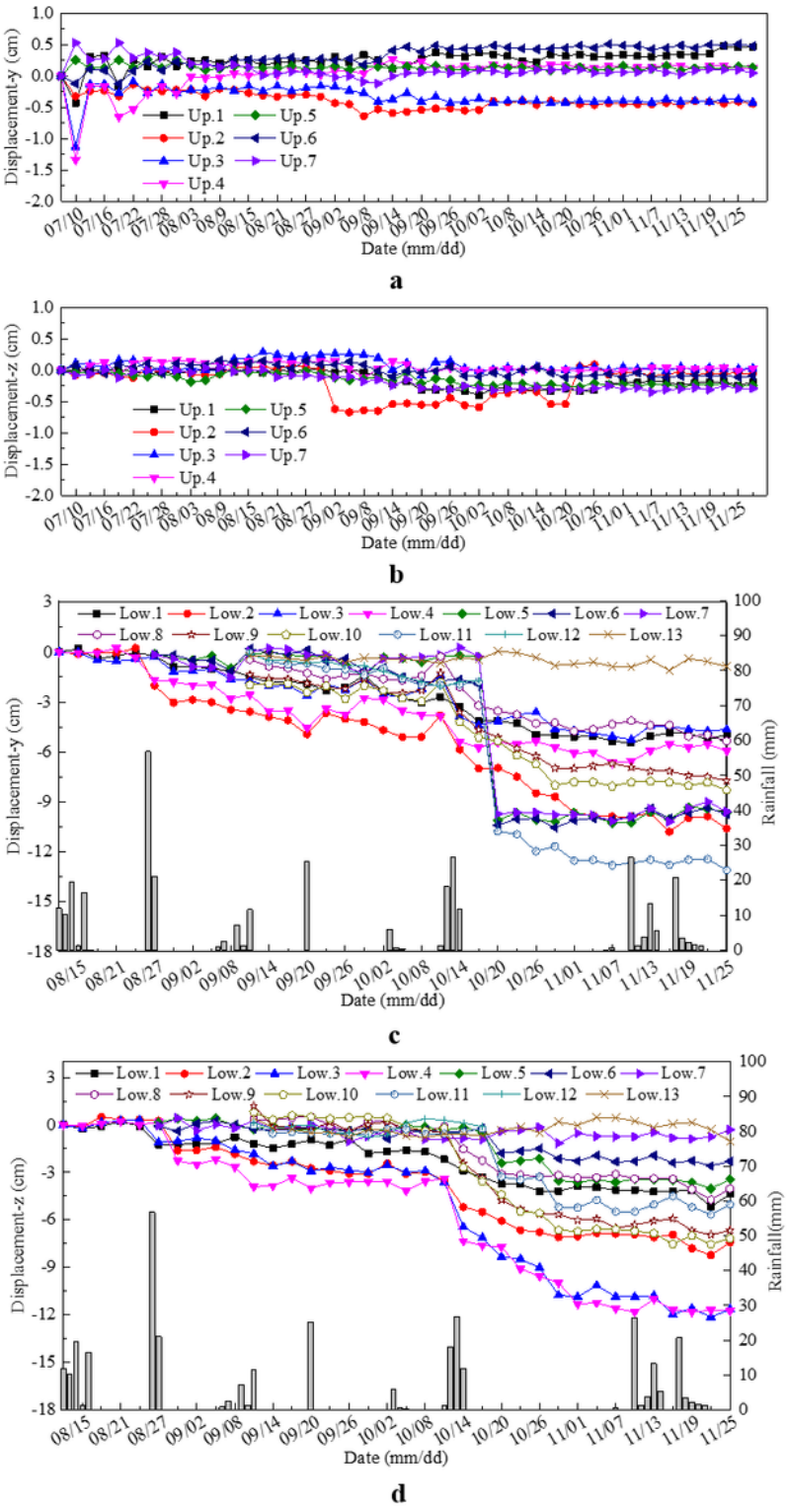

Figure 14

Monitoring results of the surface displacement points: **a** upper slope displacement vertical railway strike direction (y), **b** upper slope settlement deformation (z); **c** lower slope displacement vertical railway strike direction (y), **d** lower slope settlement deformation (z)